Experimental Validation of a Performance Model for Scarfed Nozzles

J.S. Lilley*
U.S. Army Missile Command, Redstone Arsenal, Alabama

The results of an experimental investigation into the performance of scarfed nozzles are presented. This investigation was conducted to establish the range of applicability of a performance prediction model. Factors that influence the applicability of the model are the presence of three-dimensional flow and/or boundary-layer separation. The influence of these factors on the performance of scarfed nozzles was experimentally investigated by statically firing specially designed solid rocket motors that employed various scarfed nozzle configurations. The data from these firings were used to determine applicability limits for the performance model. The results of the test program and the applicability limits obtained are presented.

Nomenclature

A = downstream throat radius attachment point
A_t = throat area
C_F = thrust coefficient
E = scarfed extension starting point
F = scarfed extension ending point, thrust
P = pressure
R^2 = correlation coefficient
X = motor axial coordinate
x = nozzle axial coordinate
Y = motor radial coordinate
y = nozzle radial coordinate
α = basic nozzle half-angle
β = scarf angle
δ = scarfed extension half-angle
ϵ = basic nozzle expansion ratio
η = thrust efficiency
θ = cant angle
ν = flow turning angle
σ = standard deviation

Subscripts

a = atmospheric
del = delivered
e = starting point scarfed extension; exit
ed = immediately downstream of shock wave
eu = immediately upstream of shock wave
f = scarfed extension ending point
min = minimum
pred = predicted
t = stagnation, chamber
X = motor axial coordinate
10% = 10% deviation limit

Superscript

$\bar{(\ )}$ = average

Received Aug. 4, 1986; revision submitted Sept. 11, 1986. This paper is declared a work of the U.S. Government and therefore is in the public domain.

*Aerospace Engineer, Propulsion Directorate. Member AIAA.

Introduction

In many existing and proposed tactical missiles, design requirements make it necessary to locate the propulsion system in the midsection of the missile. In such propulsion systems, it may be necessary to employ canted nozzles that exit through the outer skin of the missile. For aerodynamic purposes, these nozzles are typically truncated so that the exit plane of the nozzle is flush with the missile skin. This type of nozzle is commonly referred to as a scarfed nozzle.

In order to design propulsion systems that employ scarfed nozzles, development of a model to predict the performance of such nozzles is essential. The model considered in this investigation was the two-dimensional, axisymmetric performance prediction computer code developed by Hoffman.[1] Extensive theoretical and experimental investigations conducted previously[2-4] demonstrated that the model could be employed to predict scarfed nozzle performance accurately. However, no determination was made about the range of scarfed nozzle geometries and motor operating conditions for which the model was valid. Before the model could be used with a high degree of confidence, such applicability limits had to be established.

Therefore, the purpose of this investigation was to establish the range of applicability of the performance model. Two primary influences on model applicability were considered: scarfed nozzle geometry and rocket motor operating pressure. To determine influences of these two factors, several experimental tests were conducted. These tests involved the static firings of specially designed solid rocket motors that employed a variety of scarfed nozzle configurations. The data from these firings were compared against predictions from the performance model, and determinations were made about the applicability of the model.

Test Program

The performance prediction model employed in the present investigation is based on a two-dimensional axisymmetric method of characteristics flowfield solution. The validity of predictions made by the model is contingent on two major assumptions about the scarfed nozzle flowfield:

1) The flowfield throughout the nozzle (including the scarfed section) must be axisymmetric.

2) Boundary-layer separation must not occur in the scarfed section of the nozzle.

The presence of three-dimensional flowfield effects is primarily controlled by the scarfed nozzle geometry. The onset

of boundary-layer separation is controlled by both the nozzle geometry and the operating pressure of the rocket motor. Therefore, the two scarfed nozzle design factors that influence the applicability of the performance model are the scarfed nozzle geometry and the motor operating pressure.

In the performance model employed in the present investigation, the geometry of a scarfed nozzle is specified by the following parameters: half-angle of the axisymmetric section of the nozzle (basic nozzle), α; half-angle of the scarfed section of the nozzle (scarfed extension), δ; expansion ratio of the basic nozzle, ϵ; scarf angle, β; and cant angle, θ. These parameters are illustrated in Fig. 1. In most tactical missile applications, the exit plane of the nozzle is assumed to be flush with the outer skin of the missile, and as a result the scarf and cant angles are equal. In addition, the scarfed extension is assumed to be cylindrical, so δ is equal to zero. In the present investigation, the following range of scarfed nozzle geometric parameters were considered: 10 deg $\leq\alpha\leq$ 30 deg, 10 deg $\leq\beta\leq$ 30 deg, and $5\leq\epsilon\leq 20$ deg. The ranges of values were selected to be representative of scarfed nozzles employed in tactical missiles.

For the present investigation the following range of motor operating pressure, P_t, was selected for evaluation:

$$14.7 \text{ psia} \leq P_t \leq 2500 \text{ psia}$$

This pressure range ensures that, for the set of geometric parameters under consideration, both unseparated and separated flow conditions can be achieved for ambient operating conditions.

For the experimental program, the four extreme basic nozzle geometries (α, ϵ pairs) were considered for evaluation. These basic geometries were:

$$\alpha = 10 \text{ deg}, \epsilon = 5$$

$$\alpha = 30 \text{ deg}, \epsilon = 5$$

$$\alpha = 10 \text{ deg}, \epsilon = 20$$

$$\alpha = 30 \text{ deg}, \epsilon = 20$$

An experimental test series was conducted to characterize the performance of each basic nozzle geometry. In each test series, five nozzle configurations were evaluated. Each test involved a variation of the scarfed nozzle extension and/or the cant angle. To characterize the performance of the basic nozzle, one test was conducted with no cant and no extension. To evaluate the performance of a scarfed extension that had no three-dimensional flowfield effects, a second test was conducted with a nozzle that was scarfed and canted at 30 deg. A third test, to evaluate the influence of three-dimensional effects, was conducted with a nozzle that was scarfed and canted at 10 deg. Two final tests were conducted on nozzles that had unscarfed extensions and were canted at 10 deg and 30 deg respectively. The length of the nozzle extensions was equal to those of the corresponding scarfed nozzles. The purpose of these tests was to determine the relative influence of scarfing on nozzle performance. The nominal geometric specifications for the nozzles evaluated in each test series (denoted test series B-1 through B-4) are presented in Table 1. Illustrations of the general nozzle test configurations employed in test series B-1 through B-4 are presented in Fig. 2.

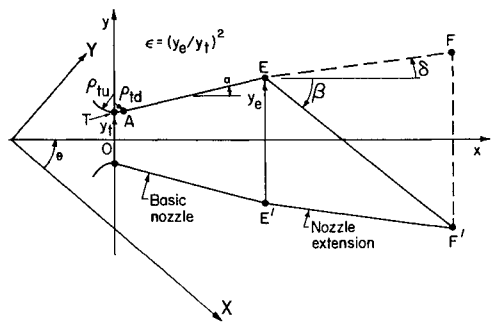

Fig. 1 Scarfed nozzle geometric model.

To evaluate the performance of the various nozzle geometries, a specially designed solid rocket motor was employed. This motor incorporated a slotted tube propellant grain designed to achieve an initial operating pressure of 2500 psia. An illustration of the propellant grain is presented in Fig. 3. Individual tests were performed by statically firing a pair of identical nozzles on one of the rocket motors. The nozzles were exhausted into still ambient air. The effects of external flow (as would be experienced under flight conditions) were not considered in this investigation. An illustration of the rocket motor assembly is presented in Fig. 4. Due to the regressive nature of the grain design, the operating pressure of the motor would continuously decrease over the duration of the burn. Consequently, during any given test, the nozzle would be subject to a range of pressures that would produce unseparated then separated operation.

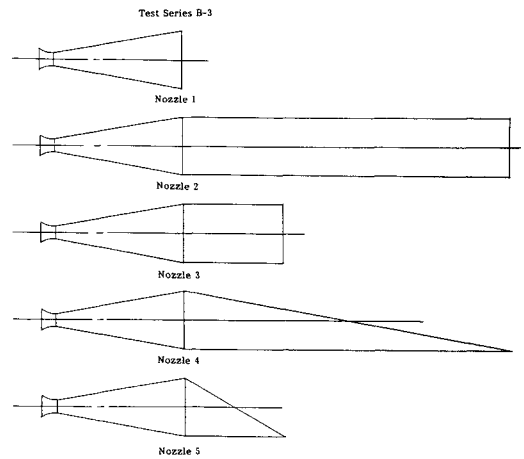

Fig. 2 Nozzle test configurations.

Table 1 Nozzle configurations for test series B-1 through B-4

Test series	Motor no.	Nozzle no.	α, deg	δ, deg	β, deg	θ, deg	ν, deg	ϵ
B-1	1	1	10	–	–	0	–	5
	2	2	10	0	90	10	10	5
	3	3	10	0	90	30	10	5
	4	4	10	0	10	10	10	5
	5	5	10	0	30	30	10	5
B-2	1	1	30	–	–	0	–	5
	2	2	30	0	90	10	30	5
	3	3	30	0	90	30	30	5
	4	4	30	0	10	10	30	5
	5	5	30	0	30	30	30	5
B-3	1	1	10	–	–	0	–	20
	2	2	10	0	90	10	10	20
	3	3	10	0	90	30	10	20
	4	4	10	0	10	10	10	20
	5	5	10	0	30	30	10	20
B-4	1	1	30	–	–	0	–	20
	2	2	30	0	90	10	30	20
	3	3	30	0	90	30	30	20
	4	4	30	0	10	10	30	20
	5	5	30	0	30	30	30	20

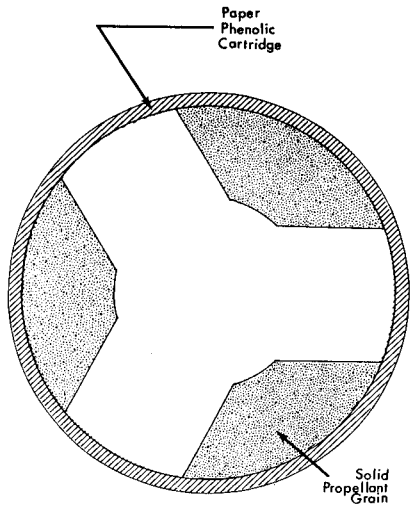

Fig. 3 Test grain cross section.

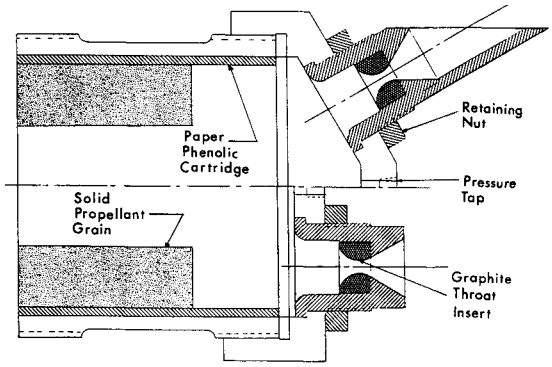

Fig. 4 Nozzle test hardware.

Test Data

Four series of experimental tests were conducted for a total of 20 nozzle tests. For each nozzle evaluation, pressure- and thrust-time histories were obtained. The thrust data were measured along the motor axis. Typical pressure-time and thrust-time histories are presented in Figs. 5 and 6, respectively. The experimentally determined values of motor axial thrust coefficient $C_{F,X}$ as a function of pressure for test series B-1 through B-4 are presented in Figs. 7–10. The definition of motor axial thrust coefficient is given by

$$C_{F,X} = \frac{F_{X,\text{del}}}{A_t P_t} \tag{1}$$

where $F_{X,\text{del}}$ is the motor axial thrust actually delivered by the motor, and A_t is the total throat area. The throat area used for each nozzle was the average value over the duration of the motor burn. This simplification was based on the fact that the average measured throat area increase due to erosion was only 3.4%.

The values of thrust efficiency η, as a function of pressure for test series B-1 through B-4, are presented in Figs. 11–14. The definition of thrust efficiency is given by

$$\eta = \frac{F_{X,\text{del}}}{F_{X,\text{pred}}} \tag{2}$$

where $F_{X,\text{pred}}$ is the motor axial thrust predicted by the performance model.[4] The predictions generated by the performance

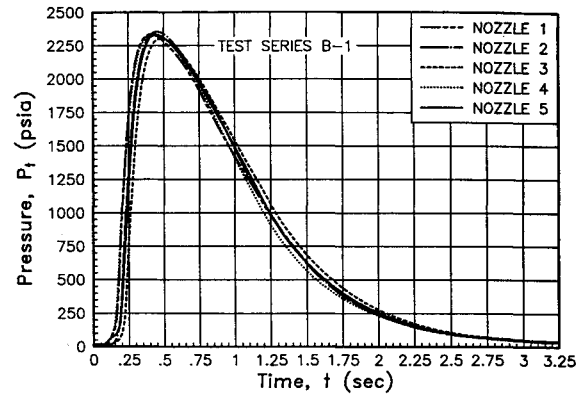

Fig. 5 Pressure vs time for test series B-1.

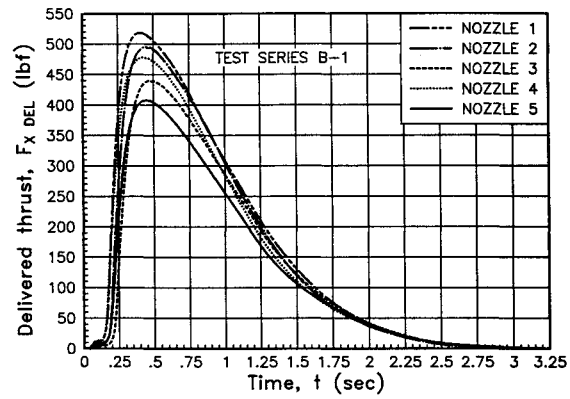

Fig. 6 Motor axial thrust vs time for test series B-1.

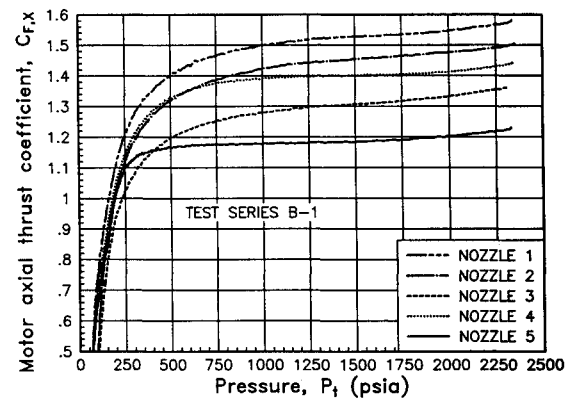

Fig. 7 Motor axial thrust coefficient as a function of pressure for test series B-1.

model, for a given nozzle, were based on the average nozzle geometry and average thermodynamic conditions over the duration of the motor burn. Justification for these simplifications are presented in detail in Ref. 5. It should be noted that all results presented in Figs. 7–14 and all subsequent calculations were based on data points generated during the regressive phase of each motor test. To avoid the influence of ignition transients, none of the data presented were taken during the portion of motor operation in which pressure and thrust were increasing with time (see Figs. 5 and 6).

Performance predictions were also made for 20 data points from each motor firing in test series B-1 through B-4. A least-squares curve fit of thrust efficiency η was performed for each

Table 2 Data correlations for test series B-1 through B-4

Test series	Motor/ nozzle	No. data points	η	R^2	$\bar{\eta}$	σ	P_t range, psia	
B-1	1	20	0.9831	0.9999	0.9821	0.005714	516	−1940
	2	20	0.9480	0.9999	0.9454	0.006737	521	−1943
	3	20	0.9685	0.9999	0.9663	0.005698	516	−1938
	4	20	0.9808	0.9996	0.9749	0.014226	497	−1932
	5	20	0.9538	0.9999	0.9512	0.005925	498	−1918
B-1	1	20	1.0132	0.9999	1.0136	0.003838	497	−2254
	2	20	0.9944	0.9990	1.0047	0.016640	505	−2247
	3	20	1.0065	0.9998	1.0059	0.007201	498	−2245
	4	20	0.9582	0.9996	0.9598	0.005027	901	−2322
	5	20	1.0084	0.9999	1.0059	0.006951	503	−2239
B-3	1	20	0.9526	0.9999	0.9528	0.001746	1247	−2197
	2	20	0.9031	0.9995	0.9019	0.003925	1255	−2201
	3	20	9.0249	0.9995	0.9236	0.004080	1249	−2196
	4	20	0.8863	0.9893	0.9832	0.013356	1580	−2366
	5	20	0.9260	0.9995	0.9249	0.003712	1244	−2199
B-4	1	20	0.9703	0.9992	0.9738	0.007343	1076	−2400
	2	20	0.9168	0.9999	0.9184	0.004614	496	−2402
	3	20	0.9539	0.9997	0.9576	0.006935	598	−2013
	4	20	0.9032	0.9959	0.9006	0.009722	1502	−2449
	5	20	0.9520	0.9989	0.9536	0.005538	1213	−2399

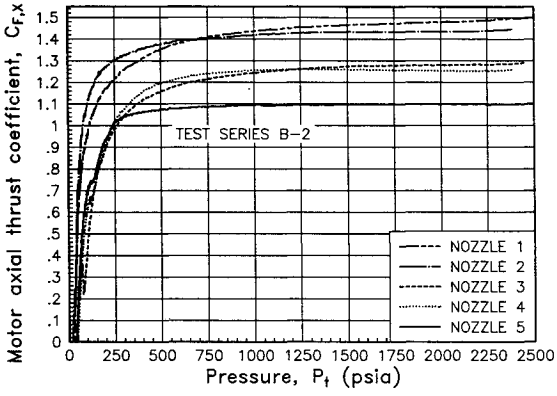

Fig. 8 Motor axial thrust coefficient as a function of pressure for test series B-2.

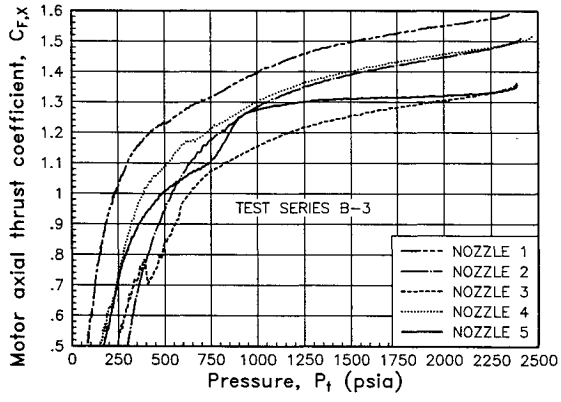

Fig. 9 Motor axial thrust coefficient as a function of pressure for test series B-3.

nozzle test along with a determination of the corresponding correlation coefficient, R^2. The relationships used to perform the curve fits are presented in Ref. 4. The results of these curve fits are presented in Table 2. The mean $\bar{\eta}$ and the standard deviation σ of the thrust efficiencies for each test and the pressure ranges for each set of data points are also presented in Table 2. The data points employed in the curve fit (when possible) were selected so that only operating pressures for which the model was valid were considered. Consequently, the least-squares thrust efficiencies presented in Table 2 were intended to be characteristic thrust efficiency values for each nozzle.

Test Results

The results of test series B-1 through B-4 were evaluated to determine the applicability of the performance model. Primary consideration was given to the influence of nozzle geometry and motor operating pressure on the predictions generated by the model.

Test Series B-1

In this test series, the basic nozzle evaluated employed a half-angle of 10 deg and a nominal expansion ratio of 5. In a previous investigation,[4,6] it was theoretically demonstrated that for a scarfed nozzle the motor axial thrust coefficient must be independent of stagnation pressure as long as the flowfield is not separated. From Fig. 7, it is evident that this result holds true for the scarfed nozzles (nozzles 4 and 5) over a wide pressure range.

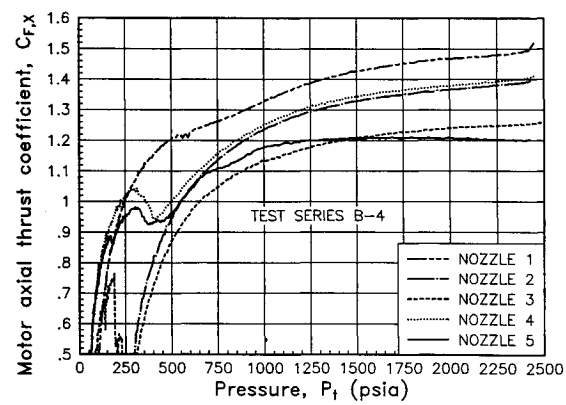

Fig. 10 Motor axial thrust coefficient as a function of pressure for test series B-4.

As shown in Fig. 11, it is evident that for each nozzle the thrust efficiency is also constant over a wide pressure range. Therefore, the assumption of using a thrust efficiency to cor-

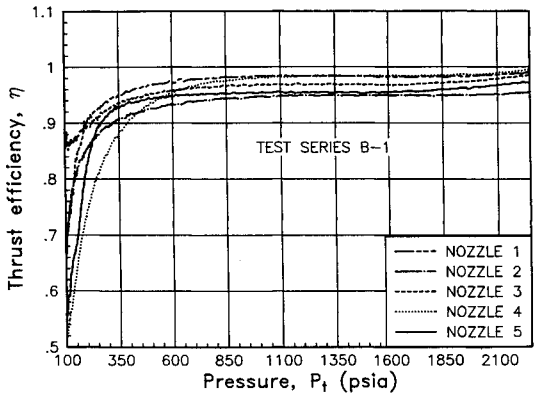

Fig. 11 Thrust efficiency as a function of pressure for test series B-1.

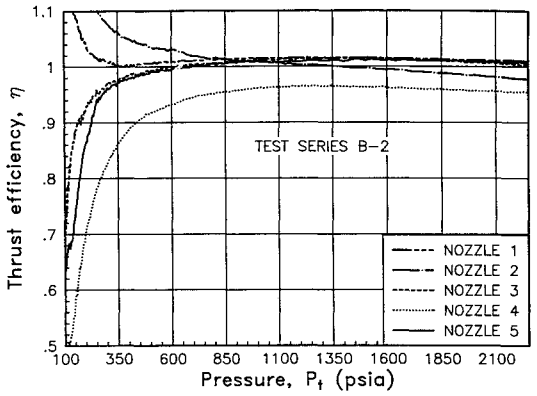

Fig. 12 Thrust efficiency as a function of pressure for test series B-2.

rect for differences between predicted and delivered performance is validated. A comparison of the thrust coefficient curves in Fig. 7 and the thrust efficiency curves in Fig. 11 clearly illustrates the ability of the model to predict nozzle performance.

Test Series B-2

In this test series, the basic nozzle evaluated employed a half-angle of 30 deg and a nominal expansion ratio of 5. The results of this test series essentially mirror those of test series B-1. Figure 8 shows that, over a wide pressure range, the motor axial thrust coefficient for each scarfed nozzle (nozzles 4 and 5) is constant. As shown in Fig. 12, the thrust efficiency for all five nozzles is constant over a wide range of pressures, further demonstrating the validity of using a thrust efficiency.

Another significant result obtained from this test series was the fact that the thrust coefficient and thrust efficiency were essentially constant for nozzle 4 (as was the case in test series B-1). For each test series, nozzle 4 was intended to demonstrate a scarfed extension for which the flowfield solution involved the presence of three-dimensional flow. The good agreement between experimental and theoretical results for nozzle 4 in both test series B-1 and B-2 demonstrates that this effect has little influence on the accuracy of the performance prediction. As a result, the overriding factor in establishing applicability limits is the onset of boundary-layer separation.

In Fig. 12 and Table 2, the values of thrust efficiency for nozzle 4 are lower than the corresponding values for the other nozzles. The primary explanation for this difference is due to a catastrophic failure that occurred during the first test of nozzle 4. As a result, the data had to be discarded and a new test conducted. To ensure maximum data uniformity within each of the test series, the intention was that all five rocket motors used were to be cast from the same propellant batch and all tests were to be fired using the same transducers and instrumentation setup. Because nozzle 4 failed in test series B-2 it was necessary to use a motor from a different propellant batch and a test setup that was not necessarily identical. This accounts for the difference in efficiency levels for nozzle 4.[5]

Test Series B-3

In this test series, the basic nozzle evaluated employed a half-angle of 10 deg and a nominal expansion ratio of 20. The results presented in Fig. 9 differ considerably from the results obtained for the previous two test series. In the case of nozzle 5, the motor axial thrust coefficient is constant over a wide pressure range; however, for nozzle 4, the thrust coefficient is never constant. Figure 13 shows that for nozzles 1–3 and 5 the thrust efficiency remains constant over a wide range of pressure, while the thrust efficiency for nozzle 4 never stabilizes.

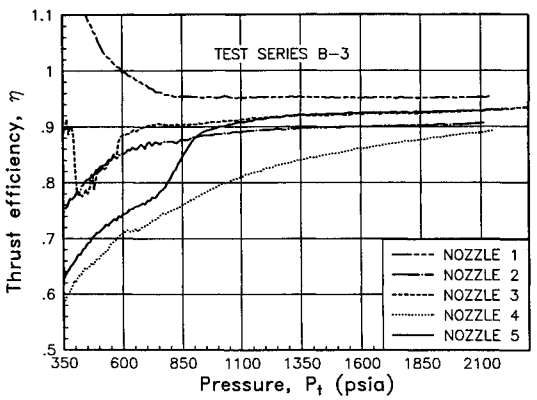

Fig. 13 Thrust efficiency as a function of pressure for test series B-3.

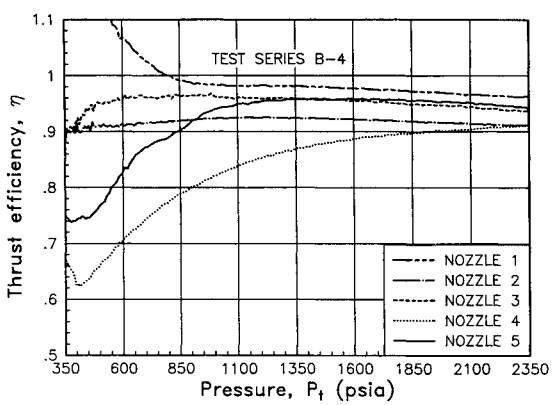

Fig. 14 Thrust efficiency as a function of pressure for test series B-4.

Test Series B-4

In this test series, the basic nozzle evaluated employed a half-angle of 30 deg and a nominal expansion ratio of 20. The results of this test series mirror those of test series B-3. Figure 10 shows that the thrust coefficient for nozzle 5 is constant over a wise pressure range, while the thrust coefficient for nozzle 4 is not constant. Figure 14 shows that all nozzles except nozzle 4, display a constant thrust efficiency over a wide pressure range.

Pressure Influence

It is evident from the test results that the presence of boundary-layer separation in the nozzle extension has a significant influence on scarfed nozzle performance. The factor that controls the separation phenomena is the static

Table 3 Nozzle pressure levels at the point of separation

Test series	Nozzle no.	$P_{t10\%}$ psia	P_{eu} psia	P_{ed} psia	P_f, psia	P_{min}, psia	P_{min}/P_a
B-1	1	168	5.41	–	–	5.41	0.3681
	2	204	6.05	11.12	6.28	4.34	0.3327
	3	180	5.37	9.86	4.34	4.34	0.2953
	4	348	10.54	19.34	11.48	8.50	0.5784
	5	225	6.94	12.71	5.62	5.62	0.3824
B-2	1	138	3.28	–	–	3.28	0.2232
	2	258	7.05	35.07	8.33	7.16	0.4872
	3	186	4.36	22.38	5.04	5.04	0.3430
	4	351	8.37	42.85	11.74	9.69	0.6594
	5	204	5.88	28.92	5.79	5.32	0.3620
B-3	1	500	2.24	–	–	2.24	0.1524
	2	474	2.12	4.70	2.10	1.79	0.1218
	3	534	2.42	5.36	2.31	2.31	0.1572
	4	>2366	>10.65	>23.58	>10.56	>9.00	>0.6124
	5	833	3.79	8.38	3.62	3.62	0.2463
B-4	1	600	2.65	–	–	2.65	0.1830
	2	298	1.36	19.81	1.20	1.61	0.1096
	3	319	1.47	10.54	1.37	1.37	0.0932
	4	>2449	>11.09	>79.94	>9.62	>9.62	>0.6546
	5	641	2.94	21.15	2.75	2.75	0.1871

pressure field in the scarfed extension and the relative magnitude of the ambient pressure. Therefore, an investigation is required into the influence of nozzle pressure levels on the applicability limits of the performance model.

To determine applicability limits for boundary-layer separation, a correlation had to be made between nozzle pressure level and the occurrence of separation. To establish this correlation, the stagnation pressure, $P_{t10\%}$, where separation occurred had to be determined for each nozzle test. The separation stagnation pressure was defined as the pressure at which the thrust efficiency deviated by more than 10% from the curve fit efficiency in Table 2, and for which the deviation exceeded 10% for the remainder of the motor burn. Determinations of the separation stagnation pressure were made for all motor firings except for nozzle 4 of test series B-3 and B-4, which were separated for the duration of the test. For these nozzles, a lower boundary on the separation pressure was determined. The respective separation pressures or separation pressure lower boundaries for each nozzle are presented in Table 3. Table 3 also contains the significant static pressure levels present in each nozzle at the separation pressure, and the ratio of the minimum static pressue to the atmospheric pressure. The static pressure levels presented in Table 3 were obtained by using the performance model to generate a flowfield analysis for each motor test.[5] The definitions of the static pressure values presented in Table 3 are:

P_{eu} = static pressure at point E upstream of the oblique shock wave
P_{ed} = static pressure at point E downstream of the oblique shock wave
P_f = static pressure at point F
P_{min} = minimum static pressure in the scarfed extension
P_a = atmospheric pressure

Note that point E is at the start of the scarfed extension and point F is at the end of the extension (see Fig. 1). Also note that an oblique shock is present at point E due to the discontinuity in the nozzle wall. The flow turning angle, which produces the shock wave, is denoted as ν. The values of ν for all nozzle tests are presented in Table 1.

Geometric Influence

In evaluating the results of test series B-1 through B-4, it is clear that there is good agreement between experimental and theoretical results, with the exception of nozzle 4 in test series B-3 and B-4. These nozzles clearly do not exhibit the expected behavior of a scarfed nozzle. The geometry of the scarfed extension in both of these nozzles is identical. The only difference in the two nozzles is the half-angle of their respective basic nozzles.

Insight into the cause of this deviation from theoretical results can be obtained from Figs. 9 and 10. It is evident that for both test series B-3 and B-4 the thrust coefficient curves for nozzles 2 and 4 are almost identical over the entire pressure range. The significance of this result is that for each test series, nozzles 2 and 4 vary in geometry only because nozzle 4 is scarfed and nozzle 2 is not. Since both nozzles employ a cylindrical extension, no nozzle axial thrust will be generated by that extension. Thus, at a given pressure level, both nozzles 2 and 4 should generate the same thrust along the nozzle axis. However, since nozzle 4 is scarfed, an additional thrust component will be generated normal to the nozzle axis. This component, normal to the nozzle axis, produces a thrust component along the missile axis. At any given pressure level, the unscarfed nozzle and the scarfed nozzle should produce different levels of motor axial thrust. The fact that nozzles 2 and 4 generate the same motor axial thrust indicates that the scarfed exension of nozzle 4 generated no thrust normal to the nozzle axis. This result would occur if the boundary layer had separated throughout the scarfed extension. The close matching of the thurst coefficients for nozzles 2 and 4 of test series B-3 and B-4 would indicate that the scarfed extension in nozzle 4 experienced boundary-layer separation over the entire pressure range evaluated.

From the results of these tests, it would seem that for the appropriate pressure ranges the model was demonstrated to be

Table 4 Scarfed nozzle separation specifications

Test series	Nozzle no.	α, deg	β, deg	ϵ	P_{min}/P_a
B-1	4	10	10	5.1309	0.5784
	5	10	30	5.0730	0.3824
B-2	4	30	10	5.1380	0.6594
	5	30	30	5.2183	0.3620
B-3	4	10	10	20.3357	>0.6124
	5	10	30	20.1611	0.2463
B-4	4	30	10	20.6040	>0.6546
	5	30	30	20.5207	0.1871

applicable for the scarf angle and half-angle values evaluated with an expansion ratio of 5. In addition, the model was shown to be applicable for the half-angle values evaluated with a scarf angle of 30 deg and an expansion ratio of 20. However, the model was not shown to be applicable for the half-angle values evaluated with a scarf angle of 10 deg and an expansion ratio of 20. The lack of agreement between theoretical and experimental result for this last set of cases does not necessarily indicate that the model is invalid for those geometries. Since the validity of the model for a given geometry is also dependent on the stagnation pressure, this result indicates that the pressure level in the nozzle was not sufficient to prevent separation.

The separation pressure levels can be employed to characterize the separation behavior of scarfed nozzles. Table 4 presents the geometric specifications of the scarfed nozzles evaluated in test series B-1 through B-4. Table 4 also includes the separation minimum pressure ratios for each of the scarfed nozzles. The results in Table 4 represent the relevant information concerning the separation behavior of the scarfed nozzles tested.

For conventional nozzles, the general guideline is that separation will occur when the minimum static pressure in the nozzle is less than 40% of the atmospheric pressure.[7] From the results in Table 4, it appears that this guideline is adequate for the number 5 nozzles but does not appear adequate for the number 4 nozzles. From the results in Table 4, it appears that a single separation guideline cannot be established for scarfed nozzles. It is evident that the geometry of the scarfed nozzle has to be considered to determine the pressure level at which separation will occur. In particular, the separation pressure ratio increases as the scarf angle decreases.

An interesting observation was made about the thrust efficiency of given nozzles after separation had occurred. In Figs. 11–14, it is evident that, for nozzle 1 in test series B-2 through B-4 and nozzle 2 in test series B-2, at pressures below the separation level, the thrust efficiency increased as the pressure decreased. This increase in thrust efficiency was a result of the reduction of the effective expansion ratio of the nozzle caused by flow separation occurring in the axisymmetric portion of the nozzle. The effective reduction in expansion ratio produced a higher than theoretical thrust coefficient, yielding a thrust efficiency greater than unity. This behavior is typical of conventional nozzles[8] and, therefore, should have occurred for all of the unscarfed nozzles (numbers 1–3) in each test series. The fact that this separation behavior did not occur consistently is difficult to explain.

Conclusions

From the results of test series B-1 through B-4, the major factors influencing the applicability of the model were identified. Over the range of nozzle geometries tested, the influence of three-dimensional flow was found to have a negligible effect on the applicability of the model. Only the presence of boundary-layer separation was determined to have a profound influence on the applicability of the model. Consequently, the nozzle stagnation pressure where separation occurred was concluded to be the major factor in determining model applicability.

From the results of the applicability limit investigations, it was determined that the performance model can yield valid predictions for the entire range of nozzle geometries encompassed by test series B-1 through B-4. This range of geometries is given by $10 \text{ deg} \leq \alpha \leq 30 \text{ deg}$, $10 \text{ deg} \leq \beta \leq 30 \text{ deg}$, $5 \leq \epsilon \leq 20$, and $\delta = 0$ deg.

Within this set of nozzle geometries, it was determined that the applicability of the model is not controlled by the particular nozzle geometry, but by the presence of boundary-layer separation. The model would be applicable for any geometry within the specified range if the pressure level in that nozzle is sufficient to prevent separation. From the results of the test progam, it was determined that, for nozzles with high scarf angles ($\beta \geq 30$ deg), separation can be prevented if the minimum static pressure in the nozzle exceeds 40% of the atmospheric pressure. It was also found that separation will be assured in nozzles with low scarf angles ($\beta \leq 10$ deg) if the minimum nozzle static pressure falls below 60% of the atmospheric pressure. In general, it is concluded that the minimum stagnation pressure for a given nozzle geometry above which the model is applicable is a function of the scarf angle. As the scarf angle increased, the minimum pressure decreased.

It should be noted that the results presented are based on static tests in which there was no external flow. For a scarfed nozzle installed in a tactical missile, flight conditions could produce a parallel external flow across the exit plane of the nozzle. At high flight velocities, this flow would influence the static pressure field in the region of the exit plane, which would in turn alter the separation behavior of the scarfed nozzle. The results presented should only be applied to flight conditions in which external flow does not influence scarfed nozzle performance (i.e., low-speed subsonic velocities).

Acknowledgments

The author wishes to express his appreciation to the personel of the Propulsion Directorate of the U.S. Army Missile Command, who provided invaluable support on this program in terms of hardware fabrication and assembly, propellant development and casting, and data acquisition and reduction.

The author wishes to express special appreciation to Albert Maykut of the Propulsion Directorate, who provided the time, resources, advice, and encouragement to allow the succcessful completion of this program.

References

[1]Hoffman, J.D., "A Computer Program for the Performance Analysis of Scarfed Nozzles," U.S. Army Missile Command, RK-CR-84-3, May 1984.

[2]Lilley, J.S. and Hoffman, J.D., "Performance Analysis of Scarfed Nozzles," AIAA Paper 84-1416, June 1984; see also Ref. 3.

[3]Lilley, J.S. and Hoffman, J.D., "Performance Analysis of Scarfed Nozzles," *Journal of Spacecraft and Rockets,* Vol. 23, Jan.-Feb. 1986, pp. 55–62.

[4]Lilley, J.S. and Hoffman, J.D., "The Analysis and Design of Scarfed Nozzles," U.S. Army Missile Command, TR-RK-85-2, Aug. 1985.

[5]Lilley, J.S., "The Analysis and Design of Propulsion Systems Employing Scarfed Nozzles," Ph.D. Dissertation, University of Alabama in Huntsville, May 1986.

[6]Lilley, J.S., "The Design and Optimizaiton of Propulsion Systems Employing Scarfed Nozzles," AIAA Paper 85-1308, 1985.

[7]Zucrow, M.J. and Hoffman, J.D., *Gas Dynamics,* Vol. 1, Wiley, New York, 1976, pp. 206–208.

[8]Sutton, G.P. and Ross, D.M., *Rocket Propulsion Elements,* Wiley, New York, 1976, pp. 66–71.